Lateral Ligand-Receptor Interactions on Membranes Probed by Simultaneous Fluorescence-Interference Detection

Martynas Gavutis, Suman Lata, Peter Lamken, Pia Müller, and Jacob Piehler

Institute of Biochemistry, Biocenter N210 Johann Wolfgang Goethe-University, 60439 Frankfurt am Main, Germany

ABSTRACT   We describe an experimental approach for studying ligand-receptor interactions in the plane of the membrane. The extracellular domains of the type I interferon receptor subunits ifnar1-EC and ifnar2-EC were tethered in an oriented fashion onto solid-supported, fluid lipid bilayers, thus mimicking membrane anchoring and lateral diffusion of the receptor. Ligand-induced receptor assembling was investigated by simultaneous total internal reflection fluorescence spectroscopy and reflectance interferometry (RIf). Based on a rigorous characterization of the interactions of fluorescence-labeled IFNα2 with each of the receptor subunits, the dynamics of the ternary complex formation on the fluid lipid bilayer was addressed in further detail making use of the features of the simultaneous detection. All these measurements supported the formation of a ternary complex in two steps, i.e., association of the ligand to ifnar2-EC and subsequent recruitment of ifnar1-EC on the surface of the membrane. Based on the ability to control and quantify the receptor surface concentrations, equilibrium, and rate constants of the interaction in the plane of the membrane were determined by monitoring ligand dissociation at different receptor surface concentrations. Using mutants of IFNα2 binding to ifnar2-EC with different association rate constants, the key role of the association rate constants for the assembling mechanism was demonstrated.

INTRODUCTION

Lateral interactions between membrane proteins play a key role for activation and propagation of cellular signaling. These lateral interactions are not static in nature and are often triggered or stabilized by interactions with further, soluble interaction partners such as ligands, effectors, and binding proteins from the matrices adjacent to the lipid bilayer. Thus, ligand-induced interaction between two or more transmembrane proteins has been recognized as the basic principle for signal transduction through receptor tyrosine kinases, (Ullrich and Schlessinger, 1990) as well as cytokine receptors (Cunningham et al., 1991). Although recent studies have challenged this model for several cytokine receptors and more complex mechanisms for interreceptor interactions have been proposed (Gent et al., 2003; Grotzinger, 2002; Remy et al., 1999; Sebald and Mueller, 2003; Stroud and Wells, 2004), simultaneous interaction of the ligand with several transmembrane proteins is still believed to be the cause of receptor activation. The interactions involved in the formation of these complexes have been characterized in solution to much detail. To conclude their consequences for signaling, a better understanding of the biophysical principles governing ligand-induced assembling of the signaling complex on the cellular membrane is needed. After ligand binding, the subsequent interactions take place in the plane of the membrane. This reduction in dimensionality has been proposed to have important physicochemical consequences (Adam and Delbruck, 1968; Axelrod and Wang, 1994; DeLisi, 1980; Vanden Broek and Thompson, 1996; Wang et al., 1992). Therefore, lateral rate and affinity constants cannot be readily deduced from the interaction parameters determined in solution. Furthermore, the coupling of ligand binding with the lateral interactions makes deconvolution of the two processes difficult as subtle interactions undetectable in bulk phase could still affect the complex formation on the surface of the membrane.

Recently, we have established detection means for assaying the interaction of type I interferons (IFNs) with their soluble receptor domains ifnar1-EC and ifnar2-EC tethered onto solid-supported membranes (Lamken et al., 2004). Although only three components are involved, the assembly process could be considerably complicated. Thus, surface-sensitive techniques suitable for deconvoluting different facets of the assembling process in real time are required. Total internal reflection fluorescence spectroscopy (TIRFS) has been frequently used for monitoring ligand binding at surfaces and solid-supported membranes (Axelrod et al., 1984; Schmid et al., 1998; Thompson et al., 1997, 1993; Thompson and Lagerholm, 1997). High sensitivity of TIRFS makes binding events detectable even at very low surface concentrations, and provides the versatility of fluorescence

Abbreviations used: ifnar, human type I interferon receptor; EC, extracellular domain; IFN, human type I interferon; wt, wild-type; tl, tagless; RIf, reflectance interferometry; TIRFS, total internal reflection fluorescence spectroscopy; SPR, surface plasmon resonance; AF488, Alexa Fluor 488; OG488, Oregon Green 488.

experiments. However, absolute quantification of the adsorbed molecules without a reference/standard is not possible. By exclusive detection of the fluorescent molecules, high signal/background ratios are achieved, but only a very limited picture of all binding events at the surface is obtained. As an alternative, label-free detection of surface-adsorbed molecules by optical techniques (Haake et al., 2000), e.g., surface plasmon resonance (SPR), grating couplers or resonant mirror, as well as by nonoptical techniques, e.g., quartz crystal microbalance (Marx, 2003) or surface acoustic waves (Gizeli et al., 1997) has been described. These techniques detect and quantify all adsorbed materials in real time, but lack the specificity and sensitivity of fluorescence detection. Thus, TIRFS would be ideally complemented with label-free detection. Combination of TIRFS with SPR (surface plasmon field-enhanced fluorescence spectroscopy) has been shown to be a powerful tool for characterizing processes at interfaces (Liebermann and Knoll, 2000; Neumann et al., 2002). This technique uses the same light source for fluorescence excitation as for SPR detection, thus limiting the flexibility of each technique. The metal layers required for SPR are furthermore disadvantageous due to their strongly surface distance-dependent fluorescence quenching.

Here, we describe a novel combination of TIRFS with reflectance interferometry (RIf) at a thin silica layer for studying lateral interactions at supported lipid bilayers. Spectral RIf has proven rugged and powerful for label-free detection of cytokine-receptor interactions (Piehler and Schreiber, 2001). The interaction of fluorescence-labeled IFNα2 with the extracellular domains of its receptor subunits ifnar1-EC and ifnar2-EC tethered onto solid-supported, fluid lipid bilayers containing chelator lipids (Dorn et al., 1998; Schmitt et al., 1994) was used as a model system. Based on simultaneous fluorescence and mass sensitive detection, we deconvoluted the interactions of this ligand with its receptor components on the lipid bilayer. Assuming a two-step kinetic complex assembling and disassembling model, we determined the association rate constant and the equilibrium dissociation constant of the lateral interaction of ifnar1-EC with IFNα2 bound to ifnar2-EC on the lipid bilayer surface. Further mechanistic aspects of receptor assembling were demonstrated by using mutants of IFNα2 binding to ifnar2-EC with different association rate constants.

MATERIALS AND METHODS

Proteins expression and purification

IFNα2, ifnar2-EC carrying a C-terminal decahistidine tag and tagless ifnar2-EC (ifnar2-tl) were expressed in *Escherichia coli*, refolded from inclusion bodies, and purified by ion exchange and size exclusion chromatography as described before (Piehler and Schreiber, 1999). In the structure of the ifnar2-EC-IFNα2 complex obtained by NMR and distance-constrained docking (Chill et al., 2003; Roisman et al., 2001), the residue S136 of IFNα2 was found proximal, yet not in contact with ifnar2-EC. This residue was mutated

to a cysteine residue for site-specific fluorescence labeling. IFNα2-S136C, IFNα2-S136CR144A, and IFNα2-S136CM148A were refolded and purified as the wt, and labeled with Alexa Fluor 488 (AF488) maleimide or Oregon Green 488 (OG488) maleimide (both from Molecular Probes, Eugene, OR). After the labeling reaction, the labeled protein was further purified by a final step of anion exchange chromatography (HiTrap Q, Amersham Biosciences, Buckinghamshire, UK), by which the fluorescence-labeled species was further enriched. In a final desalting step (HiTrap desalting, Amersham Biosciences), residual fluorescence dye was removed. Typical labeling degrees were 60–80% as estimated from the absorbance spectra. These fluorescence-labeled IFNs will be referred to as [AF488]IFNα2, [AF488]IFNα2-M148A, and [OG488]IFNα2-R144A, respectively. Ifnar1-EC with a C-terminal decahistidine tag was expressed in *Sf*9 insect cells and purified from the supernatant by immobilized metal affinity chromatography and by size exclusion chromatography as described earlier (Lamken et al., 2004). All binding assays were carried out with the glycosylated protein, which had an average molecular mass of 57 kDa as determined by mass spectrometry.

Simultaneous TIRFS-RIf detection

The experimental setup was implemented as schematically shown in Fig. 1. The beam of a 488-nm Argon ion laser (162LGA/LGL, LG Laser Technologies, Kleinostheim, Germany), equipped with an electrical shutter (Uniblitz, Vincent Associates, Rochester, NY), was coupled into a 50-μm core diameter optical fiber (Ocean Optics, Duiven, The Netherlands). Excitation power was attenuated by misaligning the laser-to-fiber coupling. The light from the fiber output was focused onto the sample surface with an adjustable collimator lens (OFR-CSMA-5-VIS, Optics for Research, Verona, NJ) through a custom-made glass prism (Berliner Glas KGaA, Berlin, Germany) with a 2.8-mm hole in the center. This hole was used for attaching the fiber optics for fluorescence detection as well as for reflectance interferometry (c.f. Fig. 1 *C*) using a custom-made optical fiber bundle (Ratioplast, Löhne, Germany), which is depicted in Fig. 1 *B*. The 600-μm fiber in the center was used for fluorescence detection. After passing an infrared cutting filter (Linos Photonics, Göttingen, Germany) the appropriate spectral range was selected with a 532-nm interference filter (Edmund Optics, Blackwood, NJ) mounted in a motorized filter wheel (AB-303, CVI Laser, Albuquerque, NM) and detected by a photomultiplier module (H7711-02, Hamamatsu, Herrsching, Germany). For reflectance interferometry, the surrounding 200-μm fibers of the fiber bundle were used: half of them were combined into a fiber bundle for illumination, whereas the other half was combined into a fiber bundle for detecting the reflected light. The transducer element (10 nm Ta_2O_5 and 400 nm silica on a glass substrate, custom-made from AMP Dünnschichttechnik GmbH, Tornesch, Germany) was optimized to give a spectral interference pattern with the inflection point at 800 nm upon perpendicular illumination (Fig. 1 *D*). White light from a tungsten halogen lamp (Avantes, Boulder, CO) was monochromatized using an 800-nm interference filter (Edmund Optics) and a 780-nm-long pass filter (LOT Oriel, Darmstadt, Germany), and was coupled into the illumination fibers. The reflected light collected by the detection fibers passed a second 800-nm interference filter (Edmund Optics) and was detected with a photomultiplier tube (H7711-02, Hamamatsu). The spectral characteristics of the detection system are shown in Fig. 1 *D*, demonstrating the strict spectral separation of fluorescence and interference signals.

The transducer was mounted to a flow cell with a 1-mm wide and 100-μm deep flow channel. Sample handling was carried out in a flow-through format using a syringe pump (Microlab 541C) with two 250-μl syringes and a four-way distribution valve (MVP) (both from Hamilton, Bonaduz, Switzerland) as in principle described before (Piehler and Schreiber, 2001), which were combined with an autosampler (PS 60, MLE GmbH, Radebeul, Germany). With this system, flow rates between 1 and 500 μl/s can be employed. Sample handling and data acquisition were controlled with software written in LabVIEW (National Instruments, Munich, Germany).
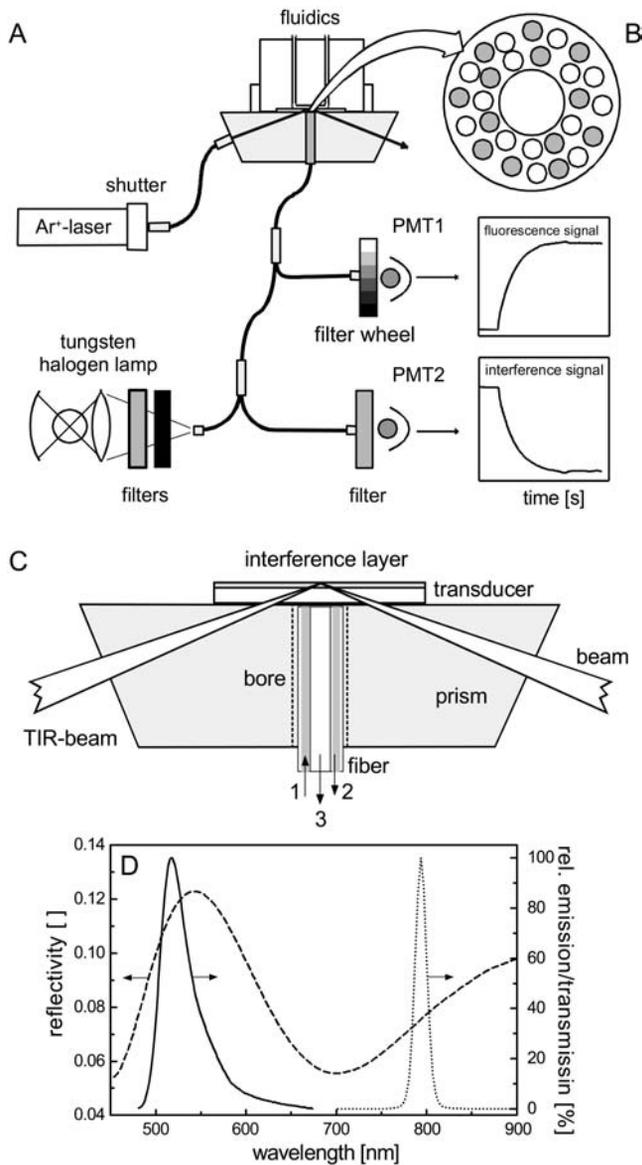
FIGURE 1 (*A*) Schematic of the setup for simultaneous TIRFS-RIf detection (details in the text). (*B*) Cross section of the fiber at the interface to the transducer: The 600-μm fiber in the center was used for fluorescence detection. The surrounding 200-μM fibers where used for RIf illumination and for RIf detection. (*C*) Enlarged view of the coupling of the light beam for fluorescence excitation into the RIf transducer, and the fibers for RIf illumination (*1*), RIf detection (*2*), and fluorescence detection (*3*). (*D*) Spectral separation of RIf and TIRFS detection: reflectivity of the RIf transducer at perpendicular illumination (*dashed line*) and transmission of the interference filter used for RIf detection (*dotted line*), in comparison to the fluorescence emission spectrum of AF488 (*solid line*).

Lipid bilayer assembling, receptor reconstitution, and binding assays

The fluorescent vesicles used for characterization of the setup were prepared by doping SOPC with the fluorescent lipids as obtained by reacting SOPE with OG488 *N*-hydroxysuccinimide ester (Molecular Probes). The lipids were homogeneously mixed in the appropriate proportion by dissolving in chloroform. The solvent was then removed in vacuo and the thin lipid film

was suspended in the buffer. The translucent solution was intermittently probe sonicated in a water bath at 4°C for 15 min followed by centrifugation to obtain small unilaminar vesicles (SUV) in the supernatant. For protein tethering to the lipid membrane, the vesicles were prepared in an identical fashion as for the fluorescent vesicles, except, SOPC was doped with 5 mol% of a chelator lipid based on a novel chelator headgroup containing two NTA moieties (termed *bis*-NTA). This chelator headgroup binds decahistidine-tagged proteins with substantially increased stability compared to the conventional *mono*-NTA, and no significant dissociation of decahistidine-tagged ifnar2-EC was detectable (i.e., $k_d < 0.0005 \text{ s}^{-1}$) even at low surface concentrations of chelator headgroups (Lata and Piehler, 2005). To avoid phase segregation, this chelator lipid contained one unsaturated alkyl chain. Its synthesis and characterization will be detailed in a forthcoming article.

Before vesicle fusion, the transducer was incubated for 30 min in a freshly prepared 2:3 mixture of two parts 30% hydrogen peroxide and three parts concentrated sulfuric acid. After extensive washing with water, the transducer was dried in a nitrogen stream and mounted immediately into the flow cell. Bilayer assembling, immobilization of the receptor domains and ligand binding assays were carried out with 20 mM HEPES, pH 7.5, and 150 mM NaCl as the running buffer. Solid supported lipid bilayers were obtained by injecting SUVs at a lipid concentration of 250 μM on the surface of the transducer. Protein immobilization and binding assays were in principle carried out as described earlier (Lamken et al., 2004). For tethering the histidine-tagged proteins to the supported membranes, the chelator headgroups were loaded with Ni^{2+}-ions by injecting 10 mM nickel(II)chloride in the running buffer for 150 s followed by a 150-s injection of 200 mM imidazole to remove nonspecifically attached lipids. Depending on the targeted surface concentrations, the histidine-tagged receptor proteins were injected at concentrations between 2 nM and 1 μM for 100–400 s. For coimmobilization of ifnar1-EC and ifnar2-EC, the proteins were injected one after the other to quantify the amount of each of the receptor components. The ligand was then injected at concentrations between 100 and 200 nM for 150 s with a flow rate of 1 μl/s, followed by a wash with 10 μl/s. Maximum flow rates of 250 μl/s were applied for measurement of fast kinetics. After a set of ligand binding experiments, all attached proteins were removed by a 150-s pulse of 200 mM imidazole, and the subsequent binding assays were carried out on the same lipid bilayer.

Data evaluation

Data were analyzed using Origin (Microcal Software), Biaevaluation 2.1 (Biacore), or Berkeley Madonna (UCB) software packages. If necessary, RIf curves were corrected for a linear drift based on the signals before tethering the proteins and after regeneration with imidazole. Different models were used for data evaluation of individual ligand-receptor interaction and for ligand binding and dissociation to ifnar1-EC and ifnar2-EC coimmobilized on supported lipid bilayers.

Pseudo-first-order binding model

Ligand binding to individual receptors was fitted with standard pseudo-first-order kinetic models for association (Eq. 1) and dissociation (Eq. 2) (Eddowes, 1987):

$$R(t) = R_{eq}\left(1 - e^{-(k_a \times c + k_d) \times (t-t_0)}\right) \quad (1)$$

$$R(t) = R_0 \times e^{-k_d \times (t-t_0)}. \quad (2)$$

$R(t)$ is the signal at time t, R_{eq} is the equilibrium signal, R_0 is the signal at $t = t_0$, k_a and k_d are association and dissociation rate constants, respectively, and c is the ligand concentration. The equilibrium dissociation constant K_D was determined from the rate constants of the interaction according to Eq. 3:

$$K_D = k_d/k_a. \quad (3)$$

Ternary complex formation and dissociation

No interactions between the extracellular domains of the receptor subunits have been detectable by several techniques (Lamken et al., 2004), and therefore preassembling of the receptor could be excluded under the experimental conditions employed in this study. Furthermore, no co-operative effect of ifnar2-EC/IFN complex formation on the IFNα2-ifnar1-EC interaction has been observed (Lamken et al., 2004). Therefore, the formation and the dissociation of the ternary complex on supported lipid bilayers was modeled as a two-step process (Whitty et al., 1998) as depicted in Fig. 2. After binding ligand of IFNα2 (L) to the high-affinity receptor ifnar2-EC (R2) on the membrane surface to form the binary IFNα2-ifnar2-EC-complex (B), ifnar1-EC is recruited by lateral interaction on the surface into the ternary complex (T). The rate constants k_a^B and k_d^B are the solution association and dissociation rate constants of the IFNα2-ifnar2-EC inter-action with the volume-related equilibrium constant K_D^B. The rate constants k_a^T and k_d^T are the surface association and dissociation rate constants, respectively, of the formation of the ternary complex from the binary complex and ifnar1-EC, and K_D^T the corresponding surface-related equilibrium dissociation constant. The following set of differential equations (as derived in more detail in the Appendix) was used for fitting the dissociation phase:

$$\frac{d[T]}{dt} = k_a^T \times [B] \times ([R1]_0 - [T]) - k_d^T \times [T]$$
$$\frac{d[B]}{dt} = -k_a^T \times [B] \times ([R1]_0 - [T]) + k_d^T \times [T] - k_d^B \times [B]$$
$$[S] = [T] + [B]. \tag{4}$$

$[R1]_0$ and $[R2]_0$ were initial surface concentrations of ifnar1-EC and ifnar2-EC, respectively. $[S]$ was the total surface concentration of the ligand, which was detected in a time-resolved manner by the TIRFS signal and converted into an absolute surface concentration using a calibration by RIf. Because $[T]$ and $[B]$ at $t = 0$ could not be parameterized, we assumed $[T] = [R2]_0$ and $[B] = 0$ as starting parameter for the fitting. Owing to the fast exchange kinetics, the actual values for $[T]$ and $[B]$ were reached within a few seconds—much faster than the dissociation of the ligand. The parameters $[R1]_0$ and $[R2]_0$ were estimated from the RIf signal of the respective experiment, whereas the values for k_d^B and k_d^T were taken from the binding assays with the individual receptors. The only fitted parameter was k_a^T. The surface dissociation constants K_D^T were determined from k_a^T and k_d^T, according to Eq. 3. Ligand association and ternary complex assembling kinetics was simulated using Eq. A5 using the experimentally determined parameters.
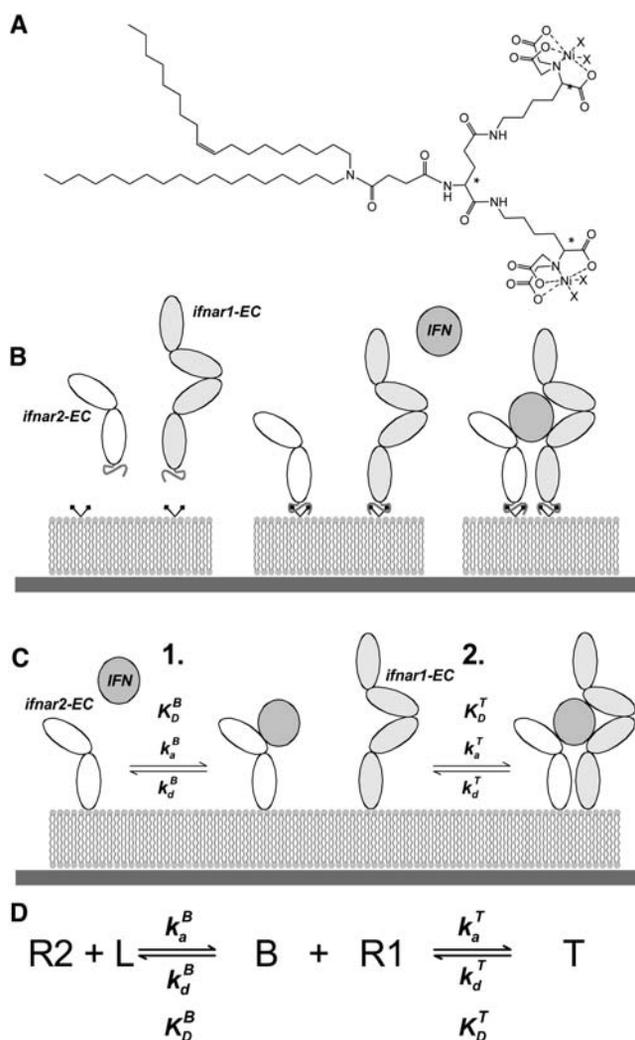

FIGURE 2 (*A*) Structure of the *bis*-NTA lipid used for tethering the extracellular receptor domains on supported lipid bilayer in a stable, yet reversible manner (*B*). (*C*) Illustration of the two-step mechanism assumed for the formation and dissociation of the ternary complex. (*D*) The corresponding interaction scheme with the identifiers used in the equations.

RESULTS

Characterization of the detection system

Solid-supported lipid bilayers are reproducibly formed by vesicle fusion on glass-type surfaces (Brian and McConnell, 1984), and have been characterized in detail with various techniques (Nagle and Tristram-Nagle, 2000; Sackmann, 1996). We therefore used lipid bilayer formation to assess the performance of TIRFS-RIf detection setup. SUVs containing OG488-labeled lipids were injected onto hydrophilic silica surfaces and fusion was monitored simultaneously on the fluorescence (TIRFS) and the interference (RIf) channels (Fig. 3 *A*). Upon a complete bilayer formation, a total de-crease of (6.7 ± 0.2) % in the light intensity was measured in the RIf channel. Assuming a surface density of 5 ng/mm^2 for a lipid bilayer (Keller and Kasemo, 1998), the RIf signal was calibrated to a mass loading of 0.7 ng/mm^2 per percentage decrease in intensity. By comparing the signals obtained for vesicle fusion by RIf and by spectral RIf, for which the mass sensitivity has been determined with radioactively labeled proteins (Hanel and Gauglitz, 2002), this mass sensitivity was also confirmed for proteins (data not shown). For clarity sake, the RIf signal converted into surface mass loading will be shown in the measurements to follow (Fig. 3 *B*). Based on this calibration, a typical rms noise of 10 pg/mm^2 was deter-mined for the RIf signal at a data acquisition rate of 1 Hz. This value is $\sim$5$\times$ higher than the rms noise of optimized spectral RIf systems under similar conditions of data acqui-sition (Piehler and Schreiber, 2001). In contrast to the un-altered RIf signal, the fluorescence signal for a full bilayer

varied with the molar fraction of the fluorescent lipids in the vesicles (Fig. 3 C). At concentrations below 1 mol%, the signal observed for a full lipid bilayer linearly correlated with the fraction of the labeled lipids. Assuming an area of 70 Å^2 per lipid molecule (Nagle and Tristram-Nagle, 2000), a detection limit of $\sim$0.1 fmol/mm^2 was reached with an excitation power of $\sim$3 μW/mm^2 (Fig. 3 D). Consequently, by increasing the excitation power, considerably lower surface concentrations than $\sim$0.1 fmol/mm^2 should be detectable. Yet all further experiments were carried out at this low a power so that the binding curves were least biased by photobleaching. For the same reason, shutter-triggered data collection was applied while monitoring slow dissociation processes. An important feature of this setup is that the two optical techniques are spectrally separated: the light intensity of the RIf channel was several orders of magnitude higher than the typical fluorescence intensity, yet no cross talk between the channels was detected. This holds true also for yellow-fluorescent dyes, which were also successfully used with this setup using a frequency-doubled Nd-YAG laser (532 nm) for excitation (data not shown).

To assess the ability of measuring transient interactions by TIRFS, the contribution of the background fluorescence from the bulk was investigated by injecting OG488 dye at different concentrations (Fig. 4 A). These experiments were carried out on solid-supported lipid bilayers containing chelator lipids. The signal from bulk fluorescence was above the noise level at dye concentrations of 200 nM and higher. The signals were fully transient and their amplitudes correlated linearly with the dye concentrations (Fig. 4 A). We used the dye injections to estimate the upper limit of the determinable rate constants. For the rise as well as the decay of the concentration in the flow cell, rate constants of $\sim$5 s^{-1} were obtained by fitting monoexponential curves (Fig. 4 B).

IFNα2 interaction with ifnar2-EC and ifnar1-EC

The interaction of wild-type IFNα2 with its receptor subunits ifnar1-EC and ifnar2-EC was previously described in detail (Lamken et al., 2004). Here, we used the IFNα2 mutant S136C with an additional cysteine, to which the fluorophore AF488 was coupled site specifically (^{AF488}IFNα2). To exclude that these modifications of the protein affected its binding properties, we characterized the interaction with each of the receptor subunits. The interaction parameters obtained from these measurements are summarized in Table 1. Fig. 5 shows TIRFS and RIf signals during the course of a typical binding assay that includes the following main steps: bilayer formation by fusion of vesicles containing 5% *bis*-NTA lipids (*1*); tethering of the high-affinity receptor component ifnar2-EC through their C-terminal decahistidine tags (*4*); binding of the fluorescently labeled ligand (*5*), and removal of the bound proteins with imidazole (*6*). Each of these steps was monitored quantitatively by RIf, confirming stable tethering of ifnar2-EC. The binding of the labeled ligand, was also detected on the TIRFS channel with substantially higher signal/noise ratio in comparison to the RIf channel. An overlay of the signals obtained by TIRFS and by RIf for the injection of ^{AF488}IFNα2 is shown in Fig. 6 A. For both the association and the dissociation phase, very similar shapes of TIRFS and RIf signals were observed. The dissociation curves were fitted by a monoexponential decay (Eq. 2) yielding a dissociation rate constant k_d of (0.010 $\pm$ 0.002) s^{-1} for both signals. An association rate constant k_a of $\sim$3 $\times$ 10^6 M^{-1}s^{-1} estimated from a monoexponential fit of the association phase (Eq. 1). Both k_a and k_d obtained for the ^{AF488}IFNα2 were in good agreement with the data obtained with wild-type IFNα2 (Lamken et al., 2004; Piehler and Schreiber, 2001) under similar experimental conditions, confirming that the mutation and the coupling of a fluorophore
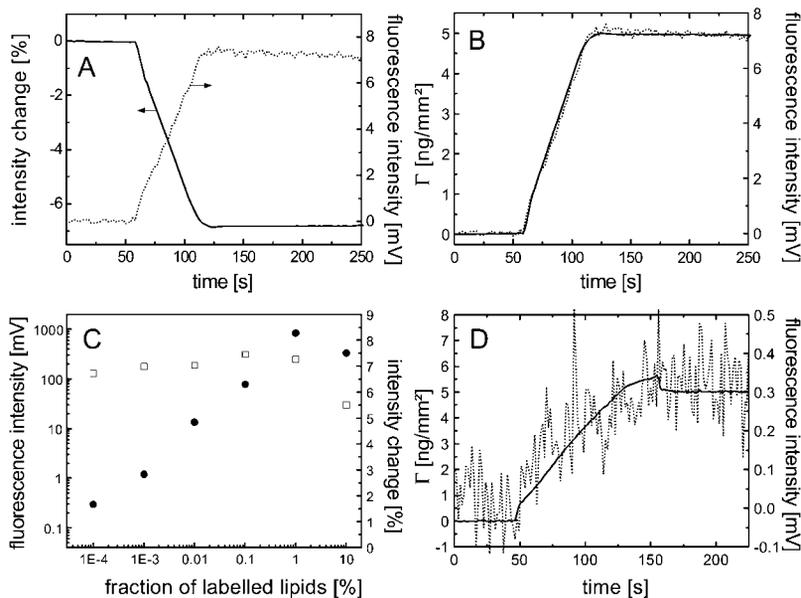

FIGURE 3 Characterization of simultaneous TIRFS-RIf detection. (*A*) Fusion of unilaminar vesicles containing fluorescently labeled lipids simultaneously detected by RIf (*solid line*) and TIRFS (*dotted line*). (*B*) Overlay of the curves shown in panel *A* after RIf intensity change was converted into surface mass deposition. (*C*) RIf ($\square$) and TIRFS ($\bullet$) signals observed for a full lipid bilayer at different fractions of labeled lipids. (*D*) RIf (*solid line*) and TIRFS (*dotted line*) signals at a fraction of 10^{-4}% fluorescent lipids.
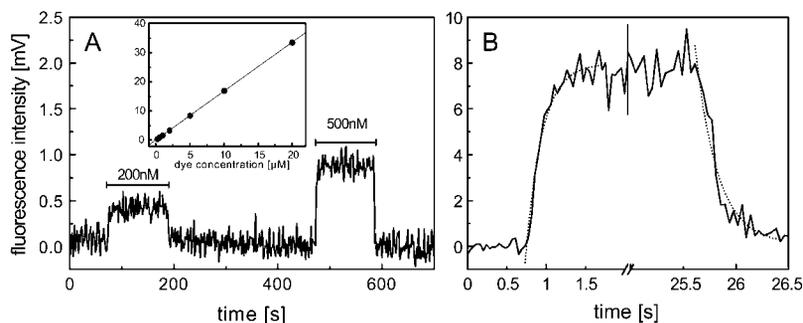
FIGURE 4 Background signals and time resolution. (*A*) Background fluorescence signals from OG488 dye in solution. The inset shows the linear dependence of the signal on the fluorophore concentration. (*B*) Concentration profile obtained from bulk fluorescence measurements and fit of the rise and decay phases by monoexponential functions.

did not affect the binding properties. However, the association and dissociation curves indicated mass transport effects, which have been frequently observed for interactions at the solid-liquid interface at high surface concentrations (Glaser, 1993; Lagerholm and Thompson, 1998; Schuck and Minton, 1996). Therefore, ligand binding at lower surface concentration of ifnar2-EC was investigated (Fig. 6 *B*), which was possible because of the higher signal/noise ratio of fluorescence detection. At ifnar2-EC surface concentrations below 150 pg/mm^2 (6 fmol/mm^2), association and dissociation phases basically unbiased by mass transport limitation were observed. Furthermore, dissociation of ^{AF488}IFNα2 in the presence of 1 μM IFNα2 was measured (Fig. 6 *C*), which gave a very similar dissociation curve as obtained at low ifnar2-EC surface concentrations (Fig. 6 *D*). From these experiments, an average k_d of 0.013 ± 0.002 s^{-1} was determined for the molecular interaction of ^{AF488}IFNα2 with ifnar2-EC. Furthermore, a strict 1:1 interaction between ifnar2-EC and IFNα2 on the lipid bilayer was confirmed. No differences in binding properties were observed between ^{AF488}IFNα2 and ^{OG488}IFNα2 (data not shown).

For the interaction of IFNα2 with ifnar1-EC, a K_D of 5 μM has been previously determined, which is three orders of magnitude higher than the K_D of the interaction of IFNα2 with ifnar2-EC (Lamken et al., 2004). Dissociation of the ligand was too fast to be resolved by RIf. Owing to a higher signal/noise ratio, dissociation of ^{AF488}IFNα2 from ifnar1-EC could be resolved by TIRFS detection at low receptor surface concentration (i.e., unbiased by rebinding). To minimize background signals, the ligand was injected at a concentration of 200 nM. The fluorescence signal upon ligand injection is shown in (Fig. 6 *C*). From these experiments, a k_d of (1 ± 0.3) s^{-1} was determined by fitting Eq. 2. Thus, the IFNα2-ifnar1-EC complex is ~100-fold less stable than the IFNα2-ifnar2-EC complex (Fig. 6 *D*). The k_a could not be reliably determined from these curves. However, a similar K_D of ~5 μM was concluded for ^{AF488}IFNα2 as for wild-type IFNα2 by comparing the equilibrium amplitudes determined by RIf at different ligand concentrations (data not shown). From these values, a k_a of ~2 × 10^5 M^{-1}s^{-1} was estimated for this interaction using Eq. 3. Thus, the ligand binds >10 times faster to ifnar2-EC than to ifnar1-EC. The same binding experiment was carried out with

^{AF488}IFNα2 in stoichiometric complex with ifnar2-tl (data not shown). A dissociation rate constant of ~1 s^{-1} was determined, confirming the similar affinity of IFNα2 and the IFNα2-ifnar2-EC complex for ifnar1-EC (Lamken et al., 2004). Thus, the interaction of ifnar2-EC with IFNα2 does not significantly affect the binding affinity of IFNα2 toward ifnar1-EC. The same binding experiments were carried out with the fluorescence labeled mutants ^{AF488}IFNα2-M148A and ^{OG488}IFNα2-R144A, which bind with altered affinity to ifnar2-EC. Also for these proteins, the S136C mutation and coupling of the fluorophore did not affect the binding properties (see below).

Ligand-induced receptor assembling

To study ligand-induced receptor assembling, both ifnar2-EC and ifnar1-EC were tethered sequentially to the lipid bilayer. The absolute amounts tethered to the surface were quantified by RIf detection. Then, 100 nM ^{AF488}IFNα2 was injected for ensuring maximum coverage of the high-affinity component ifnar2-EC, and the interaction was monitored simultaneously by RIf and TIRFS. A set of experiments with different absolute and relative surface concentrations of ifnar2-EC and ifnar1-EC is shown in Fig. 7. At high surface concentrations of both the receptor components in stoichiometric amounts (~12 fmol/mm^2), ligand dissociated very slowly (Fig. 7 *A*). When the surface concentrations of both receptor components were reduced by a factor of ~6, considerably faster dissociation was observed (Fig. 7 *B*). However, when only the surface concentration of ifnar2-EC was low (~2 fmol/mm^2), and the surface concentration of ifnar1-EC was high (~12 fmol/mm^2), the ligand dissociated at a comparably slow rate (Fig. 7 *C*). With a stoichiometric excess of ifnar2-EC on the surface, a biphasic decay with a high offset of stable-bound IFNα2 was observed (Fig. 7 *D*). The k_d of the faster decay matched the k_d of the IFNα2-ifnar2-EC interaction, whereas the remaining amount of IFNα2 confirmed a 1:1:1 stoichiometry of the complex of IFNα2 with ifnar2-EC and ifnar1-EC. The association phases for these experiments are compared in Fig. 7 *E*. Again, mass transport limitation was observed at high surface concentrations of ifnar2-EC (>4 fmol/mm^2). At low surface concentrations, the association phase perfectly matched the

TABLE 1 Parameters of the interaction with ifnar2-EC and ifnar1-EC for IFNα2 and the mutants used in this study

IFNα2*	Ifnar2-EC			Ifnar1-EC		
	k_a [M^{-1}s^{-1}]	k_d [s^{-1}]	K_D [nM]	k_d [s^{-1}]	K_D [μM]	k_a [M^{-1}s^{-1}]
wt	$(3 \pm 1) \times 10^6$	0.013 ± 0.002	4 ± 2	1 ± 0.3	~ 5	$\sim 2 \times 10^5$
M148A	$(3 \pm 1) \times 10^6$	0.3 ± 0.05	100 ± 40	1 ± 0.3	~ 5	$\sim 2 \times 10^5$
R144A	$(3 \pm 1) \times 10^5$	0.04 ± 0.005	130 ± 50	0.9 ± 0.3	~ 5	$\sim 2 \times 10^5$

*All species carried the S136C mutation and were site-specifically labeled with OG488 or AF488.

association observed for ifnar2-EC alone, and the same k_a was obtained by fitting Eq. 1.

The striking differences in the dissociation kinetics observed in these experiments support a kinetic stabilization of the ternary complex, and underscore the importance of quantifying receptor surface concentrations. The dynamic nature of the ternary complex was furthermore corroborated by challenging the ternary complex formed with ^{AF488}IFNα2 with unlabeled IFNα2 (Fig. 8 *A*). This experiment was carried out at relatively low receptor surface concentration, thus excluding bias of the dissociation kinetics by rebinding. Fast exchange of the labeled ligand was observed with much higher rate constant than the dissociation of the unchallenged ligand. Chasing with tagless ifnar2-EC did not accelerate ligand dissociation (data not shown), excluding that this effect was due to rebinding. We explain this fast exchange of the ligand by additional binding of the unlabeled ligand to unoccupied receptor subunits, which could even be detected by RIf (Fig. 8 *B*). This fast ligand exchange strongly supports a dynamic equilibrium between ternary and binary complexes.

Interaction in plane of the membrane

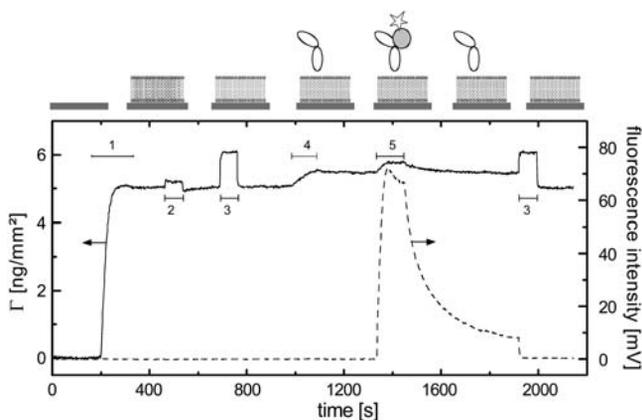With stoichiometric amounts of ifnar1-EC and ifnar2-EC, we assumed a simplified two-step mechanism for receptor

FIGURE 5 Course of a typical binding experiment on supported lipid bilayers as detected by RIf (*solid line*) and TIRFS (*dashed line*). Injection of (*1*) SOPC SUVs, (*2*) 10 mM nickel(II)chloride, (*3*) 200 mM imidazole, (*4*) 300 nM ifnar2-H10, and (*5*) 100 nM ^{AF488}IFNα2.

formation and dissociation as depicted in Fig. 2 because of the higher affinity and association rate constants of IFNα2 binding to ifnar2-EC. Under these conditions, the rate of ligand dissociation from the surface in the presence of ifnar1-EC is a probe of the dynamic equilibrium between binary (ifnar2-EC/IFNα2) and ternary complex on the membrane. We therefore determined this surface dissociation constant of this lateral interaction by evaluating ligand dissociation at various stoichiometric surface concentrations of ifnar2-EC and ifnar1-EC at stoichiometric ratio. For calculating the signals into surface concentrations, the fluorescence signal was calibrated against the mass-sensitive signal. A linear correlation of the maximum ligand binding fluorescence signals with the receptor surface concentration as determined by RIf was observed (Fig. 9 *A*). This calibration allowed: i), conversion of the fluorescence signals, as observed during ligand binding and dissociation, into mass loading (Fig. 9 *B*), and ii), precise assessment of absolute receptor surface concentrations even at low surface coverage. To determine the association rate constant k_a^T of the interaction of ifnar2-EC-bound IFNα2 with ifnar1-EC on the bilayer surface, Eq. 4 was fitted to the ligand dissociation phase with k_a^T as the only fitting parameter, whereas all the other parameters were fixed at the values determined in the previous measurements: k_d^B was parameterized with the rebinding-corrected k_d of the ifnar2-EC-IFNα2 interaction (0.013 s^{-1}); k_d^T was parameterized with the k_d of the interaction of the ligand with ifnar1-EC from solution (1 s^{-1}), assuming that tethering the complex on the membrane did not affect the complex lifetime. The receptor surface concentrations $[R1]_0$ and $[R2]_0$ were determined directly from the RIf signals. Despite the constrained parameterization, very good agreement of the fit was observed for all the measured curves (Fig. 9, *C* and *D*), which was significantly better than a monoexponential fit (Lamken et al., 2004). The k_a^T determined at different surface concentrations and the corresponding surface dissociation constant K_D^T are listed in Table 2. Strikingly, similar values for k_a^T were obtained for all dissociation curves, resulting into an average k_a^T of (16.5 ± 1.6) mm^{2}fmol^{-1}s^{-1} or ~ 0.027 μm^{2}molecules^{-1}s^{-1}. From the surface rate constants, a surface equilibrium dissociation constant K_D^T of 0.061 ± 0.006 fmol/mm^2 or ~ 36 mol/μm^2 was determined using Eq. 3.
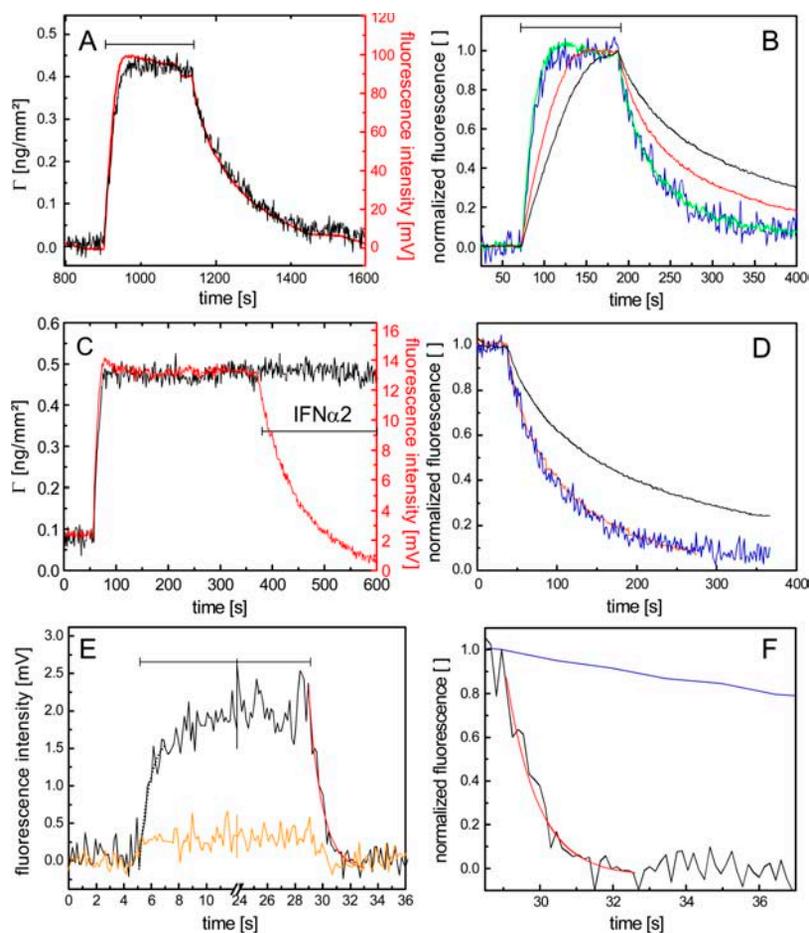
FIGURE 6 Interaction of ^{AF488}IFNα2 separately with each of the receptor subunits ifnar2-EC (A–D) and ifnar1-EC (E and F) tethered to supported lipid bilayers. (A) Ligand binding (100 nM) to ifnar2-EC and dissociation as detected simultaneously by TIRFS (red) and RIf (black). (B) Interaction of 100 nM ligand with ifnar2-EC at different ifnar2-EC surface concentrations (20 pg/mm^2, blue; 150 pg/mm^2, green; 500pg/mm^2, red; and 1000 pg/mm^2, black) as detected by TIRFS. The signals were normalized to the maximum signal, which at this ligand concentration corresponds to R_{max}. (C) Chasing of ^{AF488}IFNα2 bound to ifnar2-EC by injection of 1 μM unlabeled IFNα2 as detected by RIF TIRFS (red) and RIf (black). (D) Comparison of the dissociation curves at high ifnar2-EC surface concentration (black), at low ifnar2-EC surface concentration (blue), and for chasing with un-labeled IFNα2 (orange). (E) Binding of 200 nM ^{AF488}IFNα2 with (black) and without (orange) immobi-lized ifnar1-EC, and the fit of the dissociation curve (red). (F) Comparison of the dissociation of IFNα2 from ifnar1-EC (black) including the fit curve (red) with the dissociation from ifnar2-EC (blue).

The roles of the association rate constants

Based on these results we simulated the assembling kinetics at different receptor surface concentrations (Fig. 10 A) and different stabilities of the ligand complex with ifnar2-EC (Fig. 10 B). These simulations showed that ligand associa-tion to ifnar2-EC is the rate-determining step in ternary complex assembling (Fig. 10 A). Consequently, assembling mechanism should be primarily determined by the faster association of the ligand to ifnar2-EC compared to ifnar1-EC, and not by the stability of the complex with ifnar2-EC (Fig. 10 B). Owing to the principle of microscopic re-versibility, this faster interaction of the ligand with ifnar2-EC should also dictate the dissociation mechanism. To test this hypothesis, the dissociation from the ternary complex was probed with the mutants IFNα2-M148A and IFNα2-R144A. These mutants bind ifnar2-EC with 25–30-fold lower affinity than the wild type, but with very different rate constants (Piehler et al., 2000): for IFNα2-M148A, the k_a is unchanged compared to the wild type, whereas for IFNα2-R144A, the k_a is decreased by one order of magnitude. These mutants were site-specifically fluorescence labeled with AF488 (M148A) and OG488 (R144A) through the S136C mutation as the wild-type protein (^{AF488}IFNα2-M148A and ^{OG488}IFNα2-R144A, respectively), and the interaction with ifnar2-EC

was characterized by TIRFS-RIf detection. The dissociation of these IFNα2 mutants from ifnar2-EC are compared in Fig. 11 A. The rate constants obtained for the mutants (Table 1) were in good agreement with the published values, while binding to ifnar1-EC was unchanged compared to the wild type (data not shown).

With ifnar2-EC and ifnar1-EC coimmobilized on lipid bilayers, for both ^{OG488}IFNα2-R144 and ^{AF488}IFNα2-M148A significantly faster ligand dissociation compared to ^{AF488}IFNα2 was observed (Fig. 11 B). For ^{AF488}IFNα2-M148A, however, the dissociation at different receptor sur-face concentrations was still fitted well by the same model and the stringent parameterization as used for ^{AF488}IFNα2 (Fig. 11, C and D). Moreover, a surface association rate constant k_a^T of (18 ± 1) mm^{2}fmol^{-1}s^{-1} was obtained, resulting into a surface equilibrium dissociation constant K_D^T of 0.056 ± 0.004 fmol/mm^2 (i.e., 33 molecules/μm^2). These values are in very good agreement with the values obtained for ^{AF488}IFNα2. In contrast, considerable systematic deviation of the fit was obtained for ^{OG488}IFNα2-R144A (Fig. 11, E and F), and a significantly lower k_a^T of (9 ± 1) mm^{2}fmol^{-1}s^{-1} was obtained, resulting into a higher apparent K_D^T of 0.11 ± 0.01 fmol/mm^2. (i.e., 67 molecules/μm^2). We conclude from these results that the model shown in Fig. 2 holds true only for the
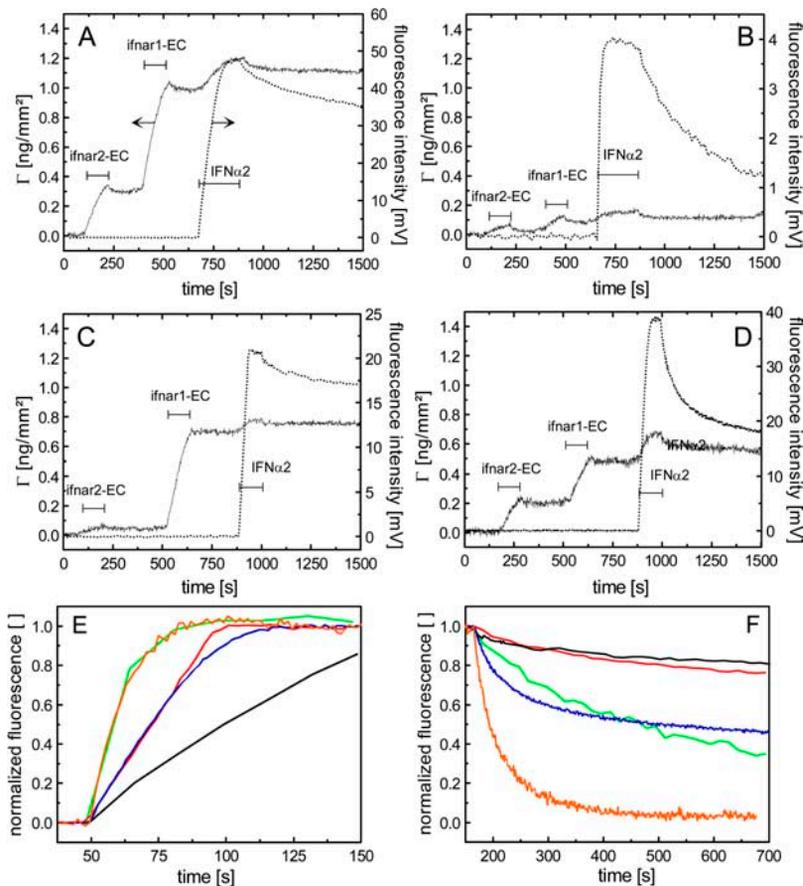
FIGURE 7 Interaction of 100 nM ^{AF488}IFNα2 with ifnar1-EC and ifnar2-EC coimmobilized onto supported lipid bilayers at different absolute and relative amounts. The signals detected by TIRFS (*dotted line*) and by RIf (*solid line*) during sequential tethering of ifnar2-EC and ifnar1-EC followed by injection of the ligand are shown in panels *A–D*. (*A*) Ifnar2-EC (25 kDa) and ifnar1-EC (57 kDa) (12 fmol/mm^2 of both). (*B*) Ifnar2-EC and ifnar1-EC (2 fmol/mm^2 of both). (*C*) Ifnar2-EC (2 fmol/mm^2)and ifnar1-EC (10 fmol/mm^2). (*D*) Ifnar2-EC (8 fmol/mm^2)and ifnar1-EC (5 fmol/mm^2). (*E* and *F*) Fluorescence traces of association (*E*) and dissociation (*F*) of ^{AF488}IFNα2 shown in panels *A* (*black*), *B* (*green*), *C* (*red*), and *D* (*blue*), in comparison to the interaction with ifnar2-EC alone (*orange*).

case that the k_a of the interaction with ifnar2-EC substantially exceeds the k_a the interaction with ifnar1-EC.

DISCUSSION

Simultaneous TIRFS-RIf detection

Precise quantification of the interacting species is a key requirement for studying biomolecular interactions in a quantitative manner. For studying protein-protein interaction on solid supported membranes, we incorporated label-free detection by RIf into a prism-based TIRFS setup. Mass-sensitive detection by RIf enabled for monitoring and quantifying all binding events on the surface including lipid bilayer fusion and receptor reconstitution, thus adding important features in comparison to exclusive fluorescence detection: i), fluorescence labeling of several components can be avoided, reducing signal cross talk and possible effects on protein function; ii), surface concentrations are directly determined and their changes are monitored, which is extremely important in case of sensitive multicomponent surface architectures; iii), straightforward calibration of fluorescence signals with respect to surface coverage. The RIf transducer element—a silica layer on top of a glass substrate—is fully transparent and does not quench surface-

proximal fluorophores, unlike noble metal surfaces required for detection by SPR, and therefore is ideally compatible with TIRFS. At the same time, its silica surface is ideally suited for preparing solid-supported fluid lipid bilayers. RIf detection is based on directional reflection, providing several advantages over other detection techniques (Hanel and Gauglitz, 2002): i), compared to evanescent field interrogation, background signals due to changes in the refractive index or buffer properties are much lower; ii), strict mass sensitivity independent on the distance from the surface or changes in shear forces; iii), simple and rugged fiber-based interrogation with no moving parts. Fluorescence excitation and emission were kept independent of RIf illumination by implementing monochromatic RIf detection in the near infrared region. Thus, we realized a simple and rugged setup for simultaneous mass sensitive and fluorescence detection without compromising the flexibility of either technique. Complete spectral separation of the two techniques proved valuable as high-power illumination for optimum RIf detection could be applied without photobleaching the fluorophores absorbing in the visible region. By further optimizing the detection, the rms noise of the RIf signal of currently 10 pg/mm^2 could be improved down to 1–2 pg/mm^2, which is comparable to spectral RIf detection (Hanel and Gauglitz, 2002). No significant cross talk be-
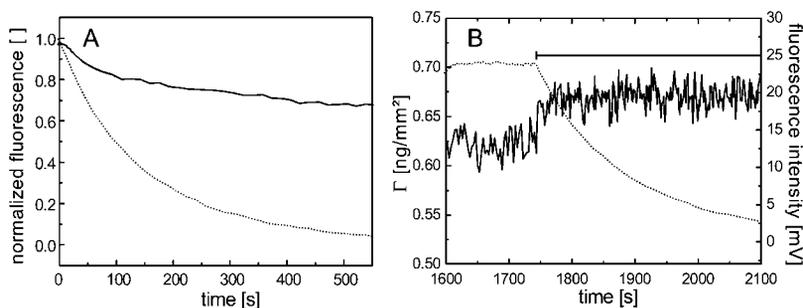
FIGURE 8 Ligand exchange in the ternary complex. Ternary complex was formed with 2 fmol/mm^2 ifnar2-EC and 10 fmol/mm^2 ifnar1-EC tethered on the lipid bilayer, followed by an injection of 100 nM ^{AF488}IFNα2. (A) Decay of the fluorescence signal in absence (solid line) and in presence (dotted line) of 10 μM unlabeled IFNα2. (B) Fluorescence (dotted line) and interference (solid line) signals during injection of 10 μM unlabeled IFNα2. Additional binding of the nonlabeled IFNα2 during this injection was detected by RIf.

tween the two techniques was detectable: fluorescence excitation with different excitation sources and different excitation power was possible without compromising RIf detection (data not shown). Vice versa, the performance of the TIRFS setup was completely independent of RIf illumination. Even at a low excitation power (2–3 μW/mm^2) a detection limit of 10^7 fluorophores/mm^2 (i.e., 10 fluorophores/μm^2) was reached, and thus fluorescence detection could be carried out without significantly photobleaching the flurophores.

Ligand-induced receptor assembling

We have applied simultaneous TIRFS-RIf detection for measuring ligand-receptor interactions within the plane of the membrane. The extracellular domains of the two subunits of the type I interferon receptor were tethered via C-terminal histidine tags in an oriented fashion onto supported lipid bilayers using chelator lipids (Dorn et al., 1998; Schmitt et al., 1994). Here, we used bis-NTA chelator headgroups,

which bind decahistidine-tagged proteins very stably (Lata and Piehler, 2005), ensuring that the interacting proteins were tightly tethered to the membrane. Thus, oriented anchoring and lateral diffusion of the receptor in the plasma membrane was mimicked while the receptor surface concentrations could be varied in a straightforward manner. Homogeneous distribution of ifnar2-EC tethered on these bilayers, and fast lateral diffusion with a diffusion coefficient of 1 μm^2/s has been previously shown by laser scanning microscopy (Lamken et al., 2004). This is comparable to the local receptor mobility on the plasma membrane as determined by single particle tracking (Ritchie et al., 2003). The formation of a complete lipid bilayer and its integrity during the experiments was monitored by RIf, thus ensuring full experimental control. Furthermore, the amounts of ifnar2-EC and ifnar1-EC tethered to the bilayers were quantified in each binding experiment. Site-specifically fluorescence-labeled IFNα2-S136C was used to dissect and study the interactions involved in ternary complex formation by monitoring ligand binding simultaneously by TIRFS and
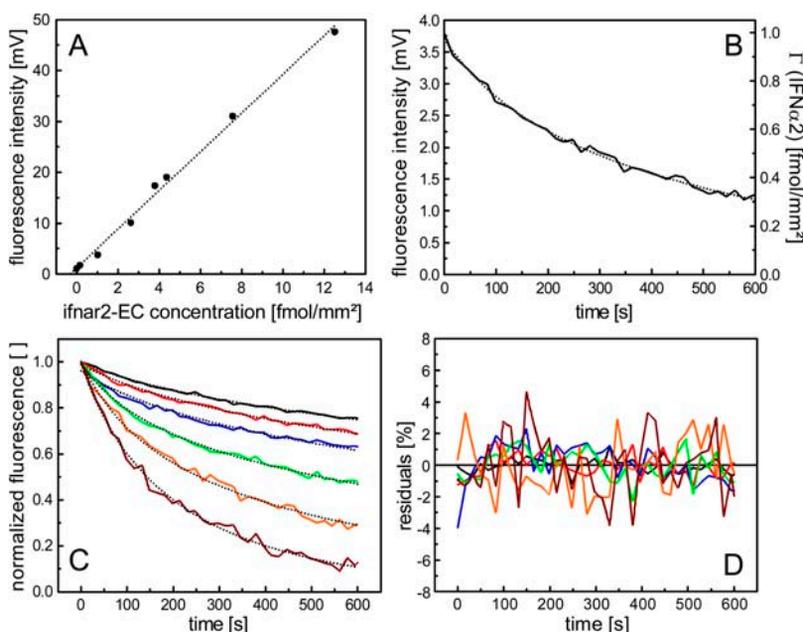

FIGURE 9 Evaluation of ligand dissociation kinetics from the ternary complex at different receptor surface concentrations. (A) Correlation between saturation ligand binding signals (fluorescence) and molar surface concentration of ifnar2-EC as determined from the RIf signal. (B) Dissociation phase at a receptor surface concentration of 1 fmol/mm^2: fluorescence signal correlated with the mass loading (solid line) and fit of Eq. 4 (dotted line). (C) Normalized dissociation phase (solid line) at different receptor surface concentrations (black, 12 fmol/mm^2; red, 8 fmol/mm^2; blue, 4 fmol/mm^2; green, 2 fmol/mm^2; orange, 1 fmol/mm^2; brown, 0.3 fmol/mm^2) with fit curves (dotted line). (D) Residuals from the curves shown in panel C (same color coding as in C).

TABLE 2 Surface association rate constants k_a^T and surface dissociation constants K_D^T determined from the fit of the ligand dissociation kinetics from the ternary complex

IFNα2	ifnar1 [fmol/mm^2]	k_a^T [mm^{2}fmol^{-1}s^{-1}]	K_D^T [fmol/mm^2]
wt	12.0	19.2	0.076
	7.8	16.8	0.047
	4.7	17.7	0.040
	3.8	16.6	0.063
	2.2	14.8	0.087
	1.0	15.5	0.085
	0.3	14.7	0.069
	Average	16 ± 2	0.061 ± 0.006
M148A	16.0	18.0	0.056
	7.4	19.0	0.053
	2.2	17.5	0.057
	Average	18 ± 1	0.056 ± 0.004
R144A	8.5	8.2	0.12
	3.9	8.5	0.12
	1.6	9.8	0.10
	Average	9 ± 1	0.11 ± 0.01

RIf. Although the interaction properties of this ligand were very similar to the interaction properties previously determined for wild-type IFNα2 (Lamken et al., 2004), we furthermore succeeded to determine the rate constants of the very transient interaction with ifnar1-EC by fluorescence detection. All results supported the previously proposed two-step assembling mechanism of the ternary complex and a dynamic equilibrium between binary and ternary complex on the membrane. Furthermore, possible cooperative effects in the ternary complex, which have been observed for other cytokine-receptor complexes, could not be detected for the IFNα2-ifnar interactions.

We used ligand dissociation kinetics for probing this dynamic equilibrium between binary and ternary complex. We assumed ligand association to ifnar2-EC as the first step (Fig. 2), thus simplifying the mathematical treatment compared to the general model (Thompson and Axelrod, 1983). The possibility of i), readily varying the receptor surface concentrations by reversible tethering, and ii), quantifying absolute surface concentrations by RIf turned out to be of key importance. Thus, we were able to precisely parameterize the system. The ligand dissociation kinetics

was fitted well by the model with a single parameter being adjusted: the association rate constant k_a^T of the interaction between the IFNα2-ifnar2-EC complex and ifnar1-EC in plane of the membrane. Despite this very constrained fitting procedure, this k_a^T turned out to be independent on the surface concentration of the receptor subunits. Even for the IFNα2-mutant M148A, which dissociated from ifnar2-EC nearly as fast as from ifnar1-EC, the ligand dissociation kinetics was properly described by the model. Strikingly, a very similar k_a^T was obtained for this mutant, confirming that the IFNα2-ifnar1-EC interaction was probed by ligand dissociation. In the case of the IFNα2-mutant R144A with a similar k_a toward ifnar2-EC and ifnar1-EC, however, the model did not properly fit the observed dissociation kinetics, and a significantly lower k_a^T was obtained as compared to IFNα2 wild type and IFNα2-M148A. These two mutants, which bind ifnar2-EC with very similar affinity, impressively demonstrate the role of the association rate constants for the assembling mechanism and the dynamics of the ternary complex on the membrane.

Interaction in two and three dimensions

The interaction of IFNα2 with ifnar1-EC in solution and on the surface can be compared based on these results: the equilibrium dissociation constant of 36 mol/μm^2 as determined for the interaction on the surface corresponds to a K_D of 5 μM (or 3000 mol/μm^3) with the ligand in solution. At the concentrations corresponding to these respective K_D, the same numbers of association events per time unit take place on the surface as in solution, assuming the same dissociation rate constants. The average distance between the molecules at these concentrations are ~200 nm on the membrane and ~100 nm in solution. Under these conditions, the probability of random collision between the two particles should be 10–100-fold higher in solution than on the membrane as estimated by the collision laws for diffusion in three and two dimensions (Hardt, 1979) taking the different diffusion coefficients in solution (~100 μm^2/s, (Kreuz and Levy, 1965) and on the membrane (1 μm^2/s) into account. Collisions must, therefore, be 10–100 times more productive when the proteins are tethered to the membrane. This substantially higher efficiency could be ascribed to a longer
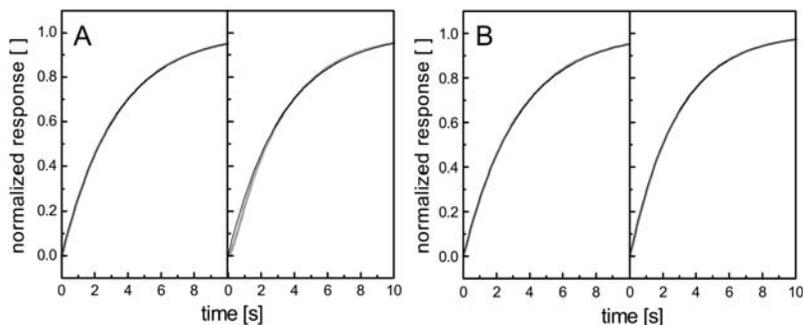

FIGURE 10 Simulation of ligand association and ternary complex formation kinetics based on the experimental rate constants of the interaction with ifnar1-EC on the membrane (ligand concentration of 100 nM). For comparison, all curves were normalized to the equilibrium signal. (A) Comparison of the ligand association kinetics (*black*) and the ternary complex formation (*gray*) at different receptor surface concentrations (*left*, 10 fmol/mm^2; *right*, 1 fmol/mm^2). (B) Comparison of the ligand association kinetics (*black*) and the ternary complex formation (*gray*) at different stabilities of the ligand interaction with ifnar2-EC (*left*, 0.01 s^{-1}; *right*, 1 s^{-1}).
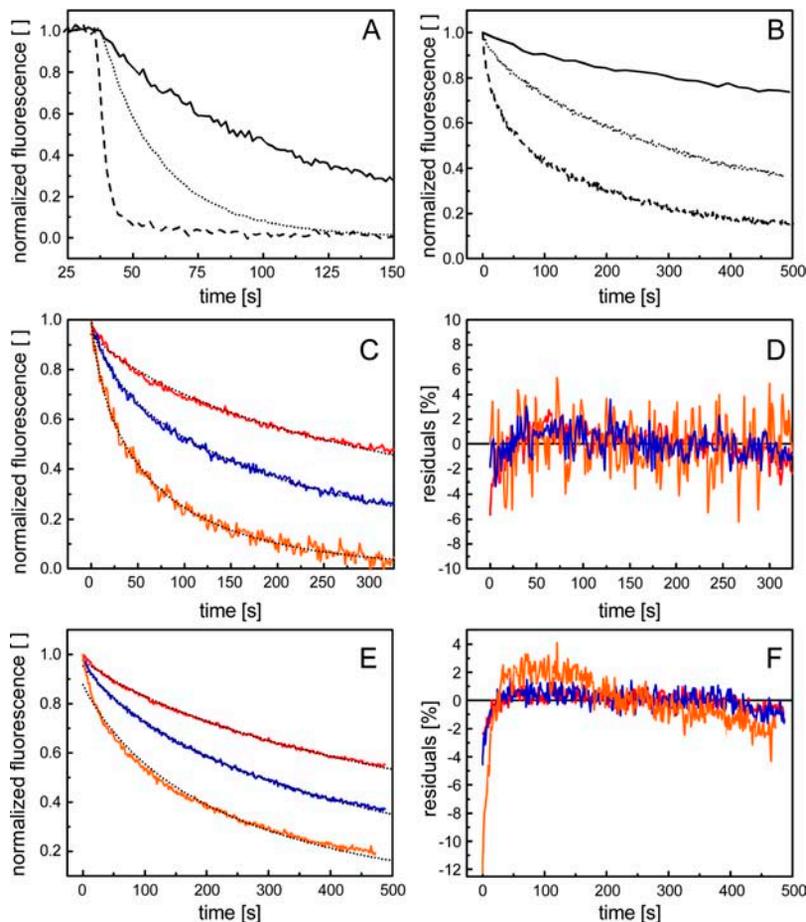
FIGURE 11 Binary and ternary complex formation analyzed for the IFNα2 mutants M148A and R144A. (*A*) Dissociation of [OG488]IFNα2-R144A (*dotted line*) and [AF488]IFNα2-M148A (*dashed line*) from ifnar2-EC in comparison to [AF488]IFNα2 (*solid line*) as detected by TIRFS. (*B*) Dissociation of [OG488]IFNα2-R144A (*dotted line*) and [AF488]IFNα2-M148A (*dashed line*) from ifnar2-EC and ifnar1-EC (both 5–7 fmol/mm^2) in comparison to [AF488]IFNα2 (*solid line*) as detected by TIRFS. (*C*) Normalized dissociation phases for [AF488]IFNα2-M148A at different receptor surface concentrations (*red*, 16 fmol/mm^2; *blue*, 7.4 fmol/mm^2; *orange*, 2.2 fmol/mm^2) with fit curves (*dotted line*). (*D*) Residuals from the curves shown in panel *C* (same color coding). (*E*) Normalized dissociation phases for [OG488]IFNα2-R144A at different receptor surface concentrations (*red*, 8.5 fmol/mm^2; *blue*, 3.9 fmol/mm^2; *orange*, 1.6 fmol/mm^2) with fit curves (*dotted line*). (*F*) Residuals from the curves shown in panel *E* (same color coding).

lifetime of the encounter complex due to slower diffusion in the membrane (Gutfreund, 1995), suggesting that a decrease in collision rate on the membrane is essentially compensated by an increase in successful collisions. Furthermore, preorientation of the membrane-tethered proteins should also contribute to higher encounter efficiency.

Receptor recruitment on the plasma membrane

Our data also implicate functional consequences, as the surface equilibrium and rate constants determine the formation and the lifetime of the ternary signaling complex. The apparent ligand dissociation rate constant (and also the apparent equilibrium dissociation constant) can be used for assessing the equilibrium on the cellular plasma membrane. Thus, 10–20% free binary complex can be estimated for IFNα2 by comparing our results with published cellular binding data (Cutrone and Langer, 1997). Indeed, very similar numbers were concluded from cellular binding data for the IL-4-receptor (Whitty et al., 1998), where the binding affinities are well comparable to the IFNα2-ifnar interaction (Letzelter et al., 1998). A surface equilibrium constant of 36 mol/μm^2, however, is not sufficient for such effective recruitment in case that the typically few 1000 receptors

are uniformly distributed on the total cell surface ($\sim$1–10 mol/μm^2). This suggests preorganization of the receptor proteins at higher local concentration within membrane domains, which have been shown to play an important role in cytokine signaling (Sehgal, 2003; Takaoka et al., 2000). The efficiency of ternary complex formation and its dynamics could well be an important parameter determining the responsiveness of different cell types. Differential responsiveness of different cells types toward different IFNs could also be explained in terms of the efficiency of recruiting ifnar1, because very different affinities have been observed for IFNα2 and IFNβ (Lamken et al., 2004).

APPENDIX

The proposed assembling mechanism shown in Fig. 2 can be described by the following set of differential equations:

$$\frac{d[T]}{dt} = k_a^T[B][R1] - k_d^T[T]$$

$$\frac{d[B]}{dt} = -k_a^T[B][R1] + k_d^T[T] - k_d^B[B] + k_a^B[R2][L], \quad \text{(A1)}$$

where [B] and [T] are the surface concentrations of the binary and the ternary complex, respectively; [R1] and [R2] are the surface concentrations of free

ifnar1-EC and ifnar2-EC, respectively; $[L]$ is the (volume) concentration of the free ligand; k_a^B and k_d^B are the association and the dissociation rate constant of ifnar2-EC-IFNα2 complex formation; k_a^T and k_d^T are the surface association and dissociation rate constants of the interaction of ifnar1-EC with the ifnar2-EC-IFNα2 complex on the surface. The total surface-bound ligand is monitored, i.e., the sum of both complexes $[S]$:

$$[S] = [T] + [B]. \tag{A2}$$

The total amount of ifnar2-EC on the membrane $[R2]_0$ is given by the sum of the amount of free ifnar2-EC, the binary complex and the ternary complex:

$$[R2]_0 = [R2] + [B] + [T]. \tag{A3}$$

The total amount of ifnar1-EC $[R1]_0$, is given by the sum of the amounts of free ifnar1-EC and the ternary complex.

$$[R1]_0 = [R1] + [T]. \tag{A4}$$

$[R1]$ and $[R2]$ from Eqs. A2 and A3 are inserted into Eq. A1:

$$\frac{d[T]}{dt} = k_a^T \times [B] \times ([R1]_0 - [T]) - k_d^T \times [T]$$
$$\frac{d[B]}{dt} = -k_a^T \times [B] \times ([R1]_0 - [T]) + k_d^T \times [T]$$
$$\qquad - k_d^B \times [B] + k_a^B \times ([R2]_0 - [T] - [B]) \times [L]$$
$$[S] = [T] + [B]. \tag{A5}$$

During dissociation ligand concentration equals 0, $[L] = 0$ and Eq. A5 can be simplified to

$$\frac{d[T]}{dt} = k_a^T \times [B] \times ([R1]_0 - [T]) - k_d^T \times [T]$$
$$\frac{d[B]}{dt} = -k_a^T \times [B] \times ([R1]_0 - [T]) + k_d^T \times [T] - k_d^B \times [B]$$
$$[S] = [T] + [B]. \tag{A6}$$

REFERENCES

Adam, G., and M. Delbruck. 1968. Reduction of dimensionality in biological diffusion processes. *In* Structural Chemistry and Molecular Biology. N. Davidson, editor. W. H. Freeman, New York, NY. 198–215.

Axelrod, D., T. P. Burghardt, and N. L. Thompson. 1984. Total internal reflection fluorescence. *Annu. Rev. Biophys. Bioeng.* 13:247–268.

Axelrod, D., and M. D. Wang. 1994. Reduction-of-dimensionality kinetics at reaction-limited cell surface receptors. *Biophys. J.* 66:588–600.

Brian, A. A., and H. M. McConnell. 1984. Allogeneic stimulation of cytotoxic T cells by supported planar membranes. *Proc. Natl. Acad. Sci. USA.* 81:6159–6163.

Chill, J. H., S. R. Quadt, R. Levy, G. Schreiber, and J. Anglister. 2003. The human type I interferon receptor. NMR structure reveals the molecular basis of ligand binding. *Structure (Camb).* 11:791–802.

Cunningham, B. C., M. Ultsch, A. M. De Vos, M. G. Mulkerrin, K. R. Clauser, and J. A. Wells. 1991. Dimerization of the extracellular domain of the human growth hormone receptor by a single hormone molecule. *Science.* 254:821–825.

Cutrone, E. C., and J. A. Langer. 1997. Contributions of cloned type I interferon receptor subunits to differential ligand binding. *FEBS Lett.* 404:197–202.

DeLisi, C. 1980. The biophysics of ligand-receptor interactions. *Q. Rev. Biophys.* 13:201–230.

Dorn, I. T., K. Pawlitschko, S. C. Pettinger, and R. Tampe. 1998. Orientation and two-dimensional organization of proteins at chelator lipid interfaces. *Biol. Chem.* 379:1151–1159.

Eddowes, M. J. 1987. Direct immunochemical sensing: basic chemical principles and fundamental limitations. *Biosensors.* 3:1–15.

Gent, J., M. Van Den Eijnden, P. Van Kerkhof, and G. J. Strous. 2003. Dimerization and signal transduction of the growth hormone receptor. *Mol. Endocrinol.* 17:967–975.

Gizeli, E., M. Liley, C. R. Lowe, and H. Vogel. 1997. Antibody binding to a functionalized supported lipid layer: a direct acoustic immunosensor. *Anal. Chem.* 69:4808–4813.

Glaser, R. W. 1993. Antigen-antibody binding and mass transport by convection and diffusion to a surface: a two-dimensional computer model of binding and dissociation kinetics. *Anal. Biochem.* 213:152–161.

Grotzinger, J. 2002. Molecular mechanisms of cytokine receptor activation. *Biochim. Biophys. Acta.* 1592:215–223.

Gutfreund, H. 1995. Kinetics for the Life Sciences: Receptors, Transmitters and Catalysts: Cambridge University Press, Cambridge, UK.

Haake, H. M., A. Schutz, and G. Gauglitz. 2000. Label-free detection of biomolecular interaction by optical sensors. *Fresenius J. Anal. Chem.* 366:576–585.

Hanel, C., and G. Gauglitz. 2002. Comparison of reflectometric interference spectroscopy with other instruments for label-free optical detection. *Anal. Bioanal. Chem.* 372:91–100.

Hardt, S. L. 1979. Rates of diffusion controlled reactions in one, two and three dimensions. *Biophys. Chem.* 10:239–243.

Keller, C. A., and B. Kasemo. 1998. Surface specific kinetics of lipid vesicle adsorption measured with a quartz crystal microbalance. *Biophys. J.* 75:1397–1402.

Kreuz, L. E., and A. H. Levy. 1965. Physical properties of chick interferon. *J. Bacteriol.* 89:462–469.

Lagerholm, B. C., and N. L. Thompson. 1998. Theory for ligand rebinding at cell membrane surfaces. *Biophys. J.* 74:1215–1228.

Lamken, P., S. Lata, M. Gavutis, and J. Piehler. 2004. Ligand-induced assembling of the type I interferon receptor on supported lipid bilayers. *J. Mol. Biol.* 341:303–318.

Lata, S., and J. Piehler. 2005. Stable and functional immobilization of histidine-tagged proteins via multivalent chelator head-groups on a molecular poly(ethylene glycol) brush. *Anal. Chem.* 77:1096–1105.

Letzelter, F., Y. Wang, and W. Sebald. 1998. The interleukin-4 site-2 epitope determining binding of the common receptor gamma chain. *Eur. J. Biochem.* 257:11–20.

Liebermann, T., and W. Knoll. 2000. Surface-plasmon field-enhanced fluorescence spectroscopy. *Colloids Surf. A.* 171:115–130.

Marx, K. A. 2003. Quartz crystal microbalance: a useful tool for studying thin polymer films and complex biomolecular systems at the solution-surface interface. *Biomacromolecules.* 4:1099–1120.

Nagle, J. F., and S. Tristram-Nagle. 2000. Structure of lipid bilayers. *Biochim. Biophys. Acta.* 1469:159–195.

Neumann, T., M. L. Johansson, D. Kambhampati, and W. Knoll. 2002. Surface-plasmon fluorescence spectroscopy. *Adv. Funct. Mater.* 12:575–586.

Piehler, J., L. C. Roisman, and G. Schreiber. 2000. New structural and functional aspects of the type I interferon-receptor interaction revealed by comprehensive mutational analysis of the binding interface. *J. Biol. Chem.* 275:40425–40433.

Piehler, J., and G. Schreiber. 1999. Biophysical analysis of the interaction of human ifnar2 expressed in E-coli with IFN alpha 2. *J. Mol. Biol.* 289:57–67.

Piehler, J., and G. Schreiber. 2001. Fast transient cytokine-receptor interactions monitored in real time by reflectometric interference spectroscopy. *Anal. Biochem.* 289:173–186.

Remy, I., I. A. Wilson, and S. W. Michnick. 1999. Erythropoietin receptor activation by a ligand-induced conformation change. *Science.* 283:990–993.

Ritchie, K., R. Iino, T. Fujiwara, K. Murase, and A. Kusumi. 2003. The fence and picket structure of the plasma membrane of live cells as revealed by single molecule techniques (Review). *Mol. Membr. Biol.* 20:13–18.

Roisman, L. C., J. Piehler, J. Y. Trosset, H. A. Scheraga, and G. Schreiber. 2001. Structure of the interferon-receptor complex determined by distance constraints from double-mutant cycles and flexible docking. *Proc. Natl. Acad. Sci. USA.* 98:13231–13236.

Sackmann, E. 1996. Supported membranes: scientific and practical applications. *Science.* 271:43–48.

Schmid, E. L., A. P. Tairi, R. Hovius, and H. Vogel. 1998. Screening ligands for membrane protein receptors by total internal reflection fluorescence: the 5-HT3 serotonin receptor. *Anal. Chem.* 70:1331–1338.

Schmitt, L., C. Dietrich, and R. Tampe. 1994. Synthesis and characterization of chelator-lipids for reversible immobilization of engineered proteins at self-assembled lipid interfaces. *J. Am. Chem. Soc.* 116:8485–8491.

Schuck, P., and A. P. Minton. 1996. Analysis of mass transport-limited binding kinetics in evanescent wave biosensors. *Anal. Biochem.* 240:262–272.

Sebald, W., and T. D. Mueller. 2003. The interaction of BMP-7 and ActRII implicates a new mode of receptor assembly. *Trends Biochem. Sci.* 28:518–521.

Sehgal, P. B. 2003. Plasma membrane rafts and chaperones in cytokine/STAT signaling. *Acta Biochim. Pol.* 50:583–594.

Stroud, R. M., and J. A. Wells. 2004. Mechanistic diversity of cytokine receptor signaling across cell membranes. *Sci. STKE.* 2004:re7.

Takaoka, A., Y. Mitani, H. Suemori, M. Sato, T. Yokochi, S. Noguchi, N. Tanaka, and T. Taniguchi. 2000. Cross talk between interferon-gamma and -alpha/beta signaling components in caveolar membrane domains. *Science.* 288:2357–2360.

Thompson, N. L., and D. Axelrod. 1983. Immunoglobulin surface-binding kinetics studied by total internal reflection with fluorescence correlation spectroscopy. *Biophys. J.* 43:103–114.

Thompson, N. L., A. W. Drake, L. Chen, and W. Vanden Broek. 1997. Equilibrium, kinetics, diffusion and self-association of proteins at membrane surfaces: measurement by total internal reflection fluorescence microscopy. *Photochem. Photobiol.* 65:39–46.

Thompson, N. L., and B. C. Lagerholm. 1997. Total internal reflection fluorescence: applications in cellular biophysics. *Curr. Opin. Biotechnol.* 8:58–64.

Thompson, N. L., K. H. Pearce, and H. V. Hsieh. 1993. Total internal reflection fluorescence microscopy: application to substrate-supported planar membranes. *Eur. Biophys. J.* 22:367–378.

Ullrich, A., and J. Schlessinger. 1990. Signal transduction by receptors with tyrosine kinase activity. *Cell.* 61:203–212.

Vanden Broek, W., and N. L. Thompson. 1996. When bivalent proteins might walk across cell surfaces. *J. Phys. Chem.* 100:11471–11479.

Wang, D., S. Y. Gou, and D. Axelrod. 1992. Reaction rate enhancement by surface diffusion of adsorbates. *Biophys. Chem.* 43:117–137.

Whitty, A., N. Raskin, D. L. Olson, C. W. Borysenko, C. M. Ambrose, C. D. Benjamin, and L. C. Burkly. 1998. Interaction affinity between cytokine receptor components on the cell surface. *Proc. Natl. Acad. Sci. USA.* 95:13165–13170.